Single-cell lymphocyte heterogeneity in advanced Cutaneous T-Cell Lymphoma skin tumors

Alyxzandria M. Gaydosik[1], Tracy Tabib[1], Larisa J. Geskin[2], Claire-Audrey Bayan[2], James F. Conway[3], Robert Lafyatis[1] and Patrizia Fuschiotti[1]*

Supplementary Materials

Supplemental Methods

Subjects and skin biopsies

Skin samples were obtained from 10 patients with a confirmed diagnosis of advanced CTCL (stage IIB-IVA), including 8 MF and 2 SS patients at the Comprehensive Skin Cancer Center, Columbia University Medical Center. Patients were well-characterized in terms of demographic, disease type, clinical features and therapy as described in Table S1. Patients were staged according to the most recent consensus, including those with leukemic blood involvement (1-6). The maximum clinical stage refers to the highest clinical stage at any point in the patient's clinical course and is not necessarily at the time of last follow-up. Mean and median number of systemic therapies was 3 (Table S1). Controls included human normal skin (NS, n=8) and atopic dermatitis (AD, n=4) obtained from The Health Sciences Tissue Bank, University of Pittsburgh. All participants gave written informed consent. Clinical information and biological specimens were de-identified and coded. Research protocols involving human subjects were approved by the Institutional Review Board of Columbia University. 6 mm biopsies of samples undergoing scRNA-seq (n=5 CTCL tumors and n=4 healthy control skin) were cut in half – one part was fixed in formalin and used for immunostaining, while the second half was used for scRNA-seq. Cell suspensions from skin were obtained as previously described (7). Briefly, skin biopsies were minced and digested enzymatically (Whole Dissociation Skin Kit, Miltenyi Biotec) for 2 hours at 37°C and further dispersed using the Miltenyi gentleMACS Octo Dissociator.

Single cell cDNA and library preparation.

Experimental procedures followed established techniques (7) using the Chromium Single Cell 3' Library V2 kit (10x Genomics). Cell suspensions were separated by the Chromium System (10X Genomics) (7,8) into mini-reaction "partitions" or GEMs formed by oil micro-droplets, each containing a gel bead and a cell. A 1000-fold excess of partitions compared to cells assured that most partitions/GEMs had only one cell per GEM. Gel beads contained an oligonucleotide scaffold composed of an oligo-dT section for priming reverse transcription, and barcodes for each cell (10X Genomics) and each transcript (unique

molecular identifier, UMI), as described (9). 7,000 cells were loaded into the instrument to obtain data on ~4,000 cells with a rate of ~3.1% of partitions showing more than one cell/partition. The following steps were all performed using reagents and protocols developed by 10X Genomics. Following GEM formation, the emulsions were transferred from the Chromium chip to a PCR cycler for cDNA synthesis. The emulsion was then broken using a recovery agent, and following Dynabead and SPRI clean up, cDNAs were amplified by PCR (C1000, Bio-Rad). cDNAs were sheared enzymatically into lengths of ~200bp. DNA fragment ends were repaired, A-tailed, and adaptors ligated. The library was quantified using the KAPA Library Quantification Kit (Illumina), and further characterized for cDNA length by bioanalyzer using a High Sensitivity DNA kit.

RNA sequencing.

RNA-seq was performed on each sample by the University of Pittsburgh Genomics Research Core (http://www.genetics.pitt.edu/our-services/rna-sequencing) using the NextSeq500 sequencing system (Illumina). Genes detected (6,000 genes/cell) had a plateau at about 200,000 reads/cell (10X Genomics, white paper). We obtained ~200 million reads/sample (NextSeq, Illumina) through the University of Pittsburgh Genomics Core, Sequencing Facility.

Data Analysis.

Chromium scRNA-seq data produced by the 10X Chromium Platform were processed to generate sample-specific fastq files. Processed reads were then examined by quality metrics, mapped to a reference human genome using RNA-seq aligner STAR and assigned to individual cells of origin according to the cell specific barcodes, using the Cell Ranger pipeline (10X Genomics). To ensure that PCR amplified transcripts were counted only once, only single UMIs were counted for gene expression level (10). In this way, cell x gene UMI counting matrices were generated for downstream analyses. Seurat, an R package developed for single-cell analysis (11), was used to identify distinct cell populations and visualize cell clusters in graphs as in (8). Specifically, the UMI matrix was filtered such that only cells expressing at least 200 genes were utilized in downstream analysis. Unwanted sources of variation were

regressed out of the data by constructing linear models to predict gene expression based on the number of UMIs per cell as well as the percentage of mitochondrial gene content. Based on their average expressions and dispersions, 4,451 highly variable genes were identified and principal component analysis (PCA) was subsequently performed on the scaled data of the identified highly variable genes. Statistically significant PCs were identified using a resampling test inspired by Jackstraw (12). Cells were clustered using Seurat (11) (Louvain clustering). The resultant clusters were then visualized using a t-distributed stochastic neighbor embedding (t-SNE) projection plot (13). For gene differential tests, we used the "FindAllMarkers" package, which uses the Wilcoxon rank sum test to show differential genes with a minimum percentage of cells of 25% per cluster.

Cell cycle analysis.

Cell cycle scoring of lymphocytes from tumor and control samples was obtained using the guidelines outlined by Satija and Hoffman (11). Briefly, canonical markers were used to determine the phase of cell cycle. A list of gene markers derived from Tirosh *et al*. (14) were separated into markers of G2/M phase and markers of S phase. Cell cycle scores were assigned based on the expression of these markers, with cells lacking expression of genes from either marker set assumed to be non-cycling (G1 phase).

Multicolor immunohistochemistry

Single and dual antibody staining using tyramide signal amplification (ThermoFisher) were performed on formalin-fixed, paraffin-embedded skin samples as previously described (7). The Antibodies used in these experiments were all purchased from Sigma. Immunohistochemistry images were obtained with an Evos FL Auto microscope (Life Technologies). Confocal images were captured on an Olympus Fluoview 1000 confocal microscope using an oil immersion 100X objective.

Bibliography

1. Olsen E, Vonderheid E, Pimpinelli N, Willemze R, Kim Y, Knobler R*, et al.* Revisions to the staging and classification of mycosis fungoides and Sezary syndrome: a proposal of the International Society for Cutaneous Lymphomas (ISCL) and the cutaneous lymphoma task force of the

European Organization of Research and Treatment of Cancer (EORTC). Blood **2007**;110(6):1713-22 doi blood-2007-03-055749 [pii]

2. Olsen EA, Whittaker S, Kim YH, Duvic M, Prince HM, Lessin SR*, et al.* Clinical end points and response criteria in mycosis fungoides and Sezary syndrome: a consensus statement of the International Society for Cutaneous Lymphomas, the United States Cutaneous Lymphoma Consortium, and the Cutaneous Lymphoma Task Force of the European Organisation for Research and Treatment of Cancer. J Clin Oncol **2011**;29(18):2598-607 doi JCO.2010.32.0630 [pii]
3. Vonderheid EC, Bernengo MG, Burg G, Duvic M, Heald P, Laroche L*, et al.* Update on erythrodermic cutaneous T-cell lymphoma: report of the International Society for Cutaneous Lymphomas. J Am Acad Dermatol **2002**;46(1):95-106 doi S0190962202413266 [pii].
4. Scarisbrick JJ, Kim YH, Whittaker SJ, Wood GS, Vermeer MH, Prince HM*, et al.* Prognostic factors, prognostic indices and staging in mycosis fungoides and Sezary syndrome: where are we now? Br J Dermatol **2014**;170(6):1226-36 doi 10.1111/bjd.12909.
5. Scarisbrick JJ, Prince HM, Vermeer MH, Quaglino P, Horwitz S, Porcu P*, et al.* Cutaneous Lymphoma International Consortium Study of Outcome in Advanced Stages of Mycosis Fungoides and Sezary Syndrome: Effect of Specific Prognostic Markers on Survival and Development of a Prognostic Model. J Clin Oncol **2015** doi 10.1200/JCO.2015.61.7142.
6. Desai M, Liu S, Parker S. Clinical characteristics, prognostic factors, and survival of 393 patients with mycosis fungoides and Sezary syndrome in the southeastern United States: a single-institution cohort. J Am Acad Dermatol **2015**;72(2):276-85 doi 10.1016/j.jaad.2014.10.019.
7. Tabib T, Morse C, Wang T, Chen W, Lafyatis R. SFRP2/DPP4 and FMO1/LSP1 Define Major Fibroblast Populations in Human Skin. The Journal of investigative dermatology **2018**;138(4):802-10 doi 10.1016/j.jid.2017.09.045.
8. Macosko EZ, Basu A, Satija R, Nemesh J, Shekhar K, Goldman M*, et al.* Highly Parallel Genome-wide Expression Profiling of Individual Cells Using Nanoliter Droplets. Cell **2015**;161(5):1202-14 doi 10.1016/j.cell.2015.05.002.

9. Zheng GX, Terry JM, Belgrader P, Ryvkin P, Bent ZW, Wilson R*, et al.* Massively parallel digital transcriptional profiling of single cells. Nature communications **2017**;8:14049 doi 10.1038/ncomms14049.
10. Islam S, Zeisel A, Joost S, La Manno G, Zajac P, Kasper M*, et al.* Quantitative single-cell RNA-seq with unique molecular identifiers. Nat Methods **2014**;11(2):163-6 doi 10.1038/nmeth.2772.
11. Satija R, Farrell JA, Gennert D, Schier AF, Regev A. Spatial reconstruction of single-cell gene expression data. Nat Biotechnol **2015**;33(5):495-502 doi 10.1038/nbt.3192.
12. Chung NC, Storey JD. Statistical significance of variables driving systematic variation in high-dimensional data. Bioinformatics **2015**;31(4):545-54 doi 10.1093/bioinformatics/btu674.
13. van der Maarten L, Hinton G. Visualizing Data using t-SNE. Journal of Machine Learning Research **2008**;9:2579-29605.
14. Tirosh I, Izar B, Prakadan SM, Wadsworth MH, 2nd, Treacy D, Trombetta JJ*, et al.* Dissecting the multicellular ecosystem of metastatic melanoma by single-cell RNA-seq. Science **2016**;352(6282):189-96 doi 10.1126/science.aad0501.
15. Geskin LJ, Viragova S, Stolz DB, Fuschiotti P. Interleukin-13 is over-expressed in cutaneous T-cell lymphoma cells and regulates their proliferation. Blood **2015** doi blood-2014-07-590398 [pii]

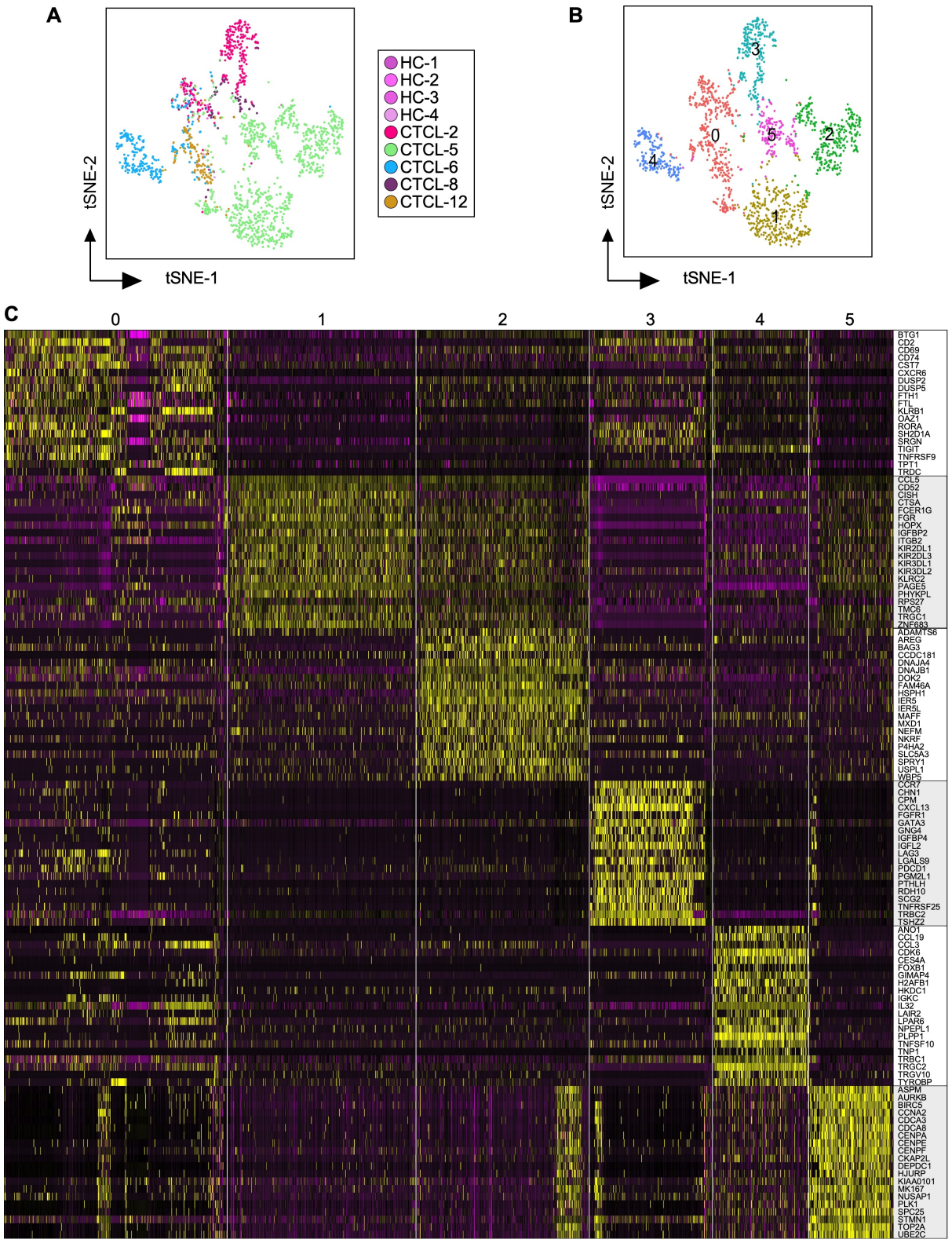

Supplementary Figure 1. (A) Transcriptomes of TOX^{+} T lymphocytes from individual CTCL tumors and normal skin samples (color coded by subject), revealing 6 discrete Louvain clusters **(B)**. **(C)** Heat map showing examples of the most highly significant differentially expressed genes (n=20) for each cluster from (B). Cluster numbers are indicated at the top, while the cell source is indicated on the right side. Each column represents a cell.

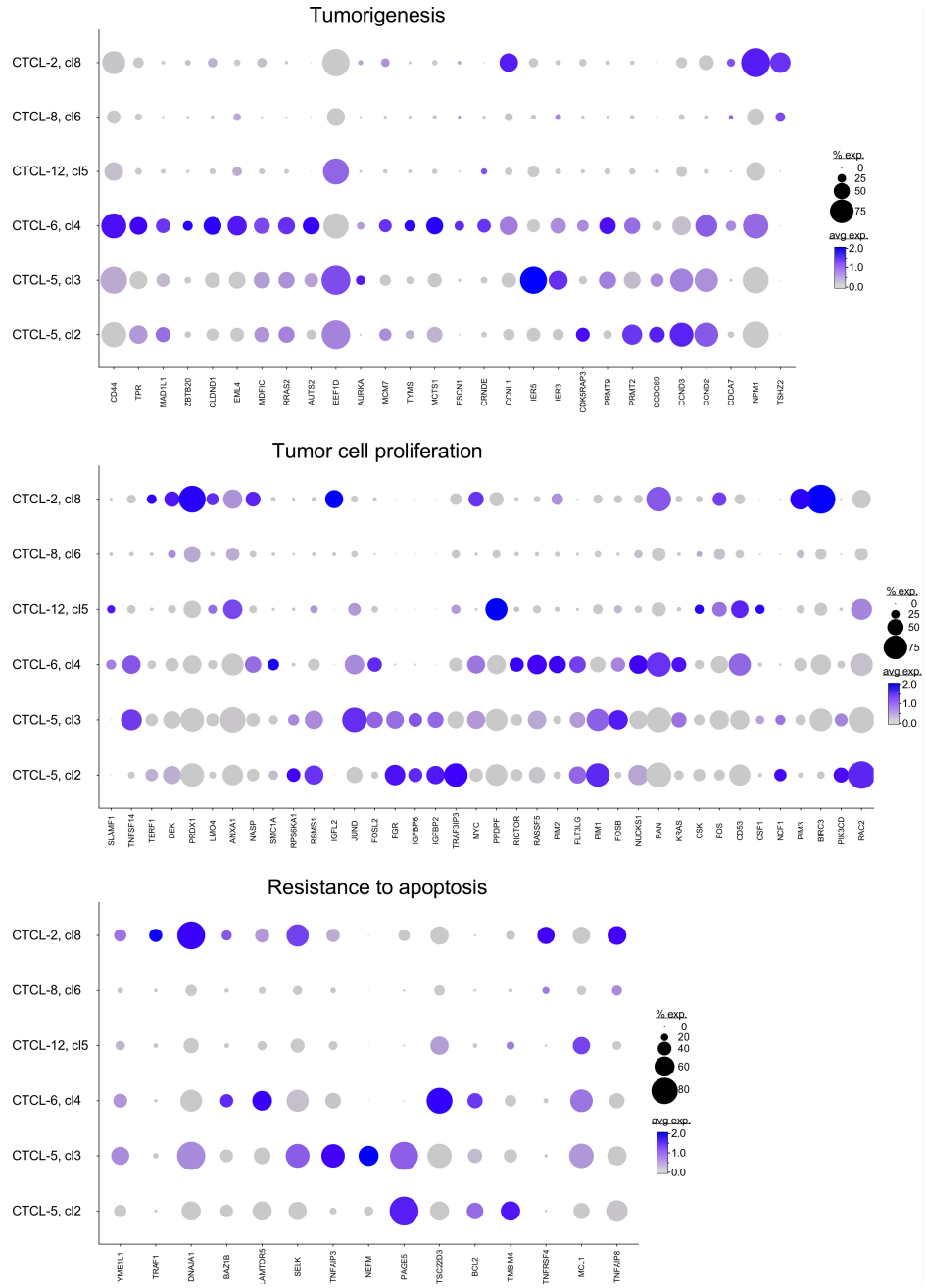

Supplementary Figure 2. Dot-plots showing the proportion of cells and the scaled average gene expression of the DE genes associated with tumorigenesis, tumor-cell proliferation, and resistance to apoptosis. Some examples of genes that are uniquely expressed in these tumor-specific clusters include TRAF1, PIM3, BIRC3, IGFL2 (CTCL-2), RPS6KA1, FGR, IGFBP6/P2, PIM1, NCF1, IER5, CCDC69, CCND3, PIK3CD, TNFAIP3, NEFM, PAGE5 (CTCL-5), SMC1A, ZBTB20, FSCN1, RICTOR (CTCL-6) and PPDPF, CSK, PRDM1, NTRK2 (CTCL-12).

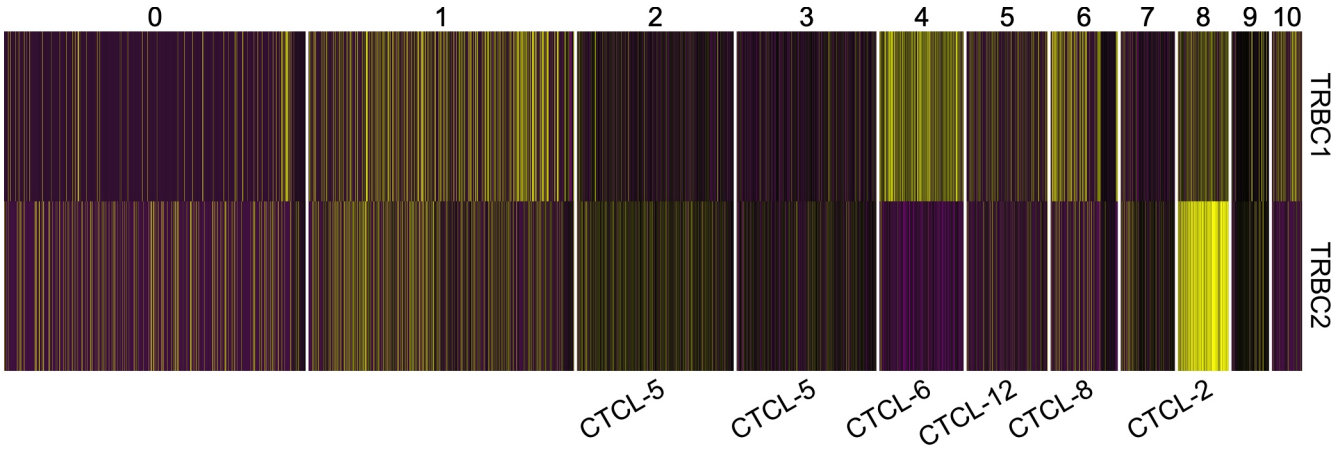

Supplementary Figure 3. Differential expression of TRBC1 and TRBC2 by lymphocytes from CTCL tumor and normal skin samples in Louvain clusters 0 to 10 of Fig. 2C. Cluster numbers are indicated at the top, while the tumor-specific clusters are indicated at the bottom. Each column represents a cell.

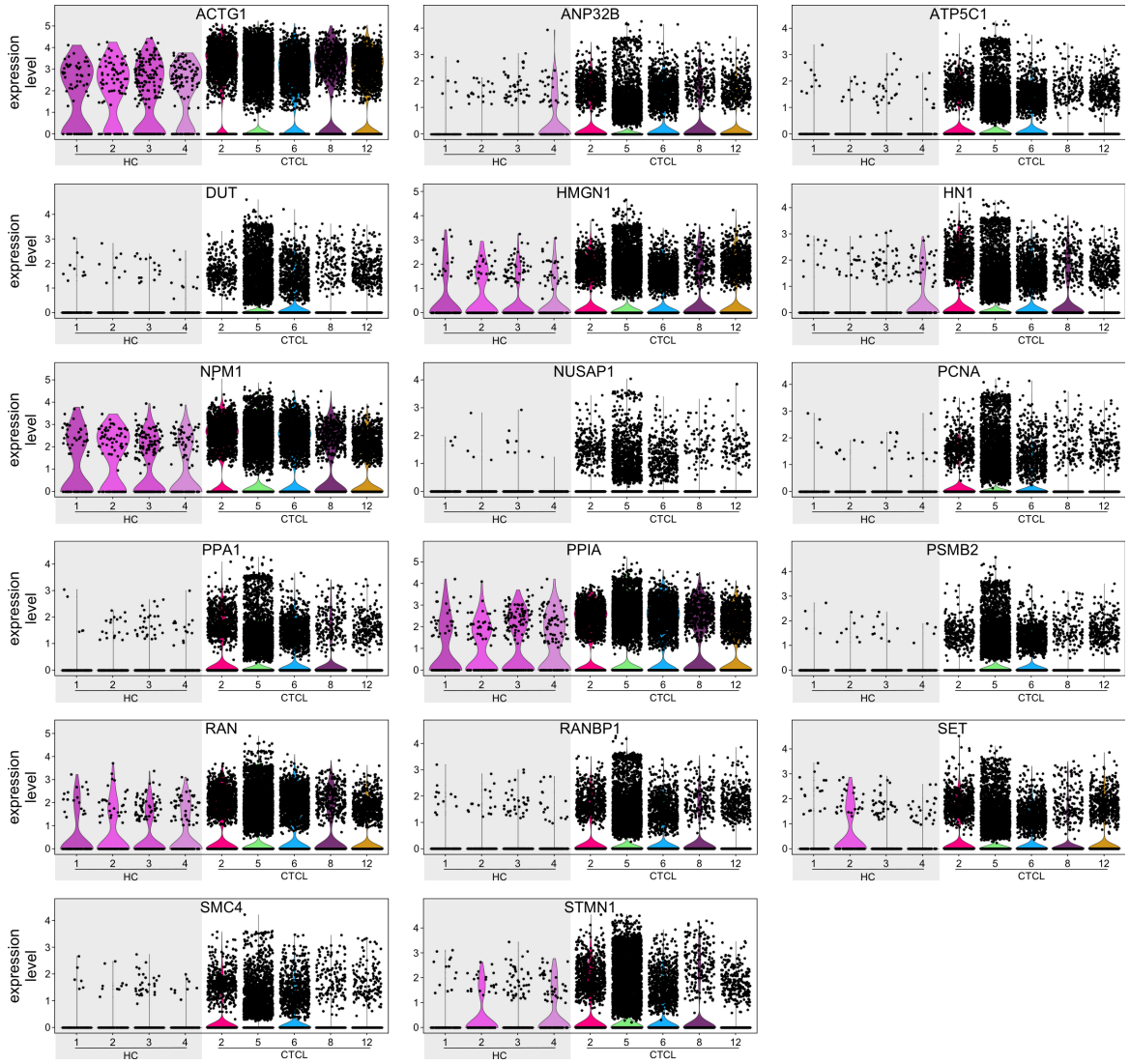

Supplementary Figure 4. Violin plots showing expression levels of 17 genes common to the highly proliferating T-lymphocytes from tumor samples (Fig. 3D).

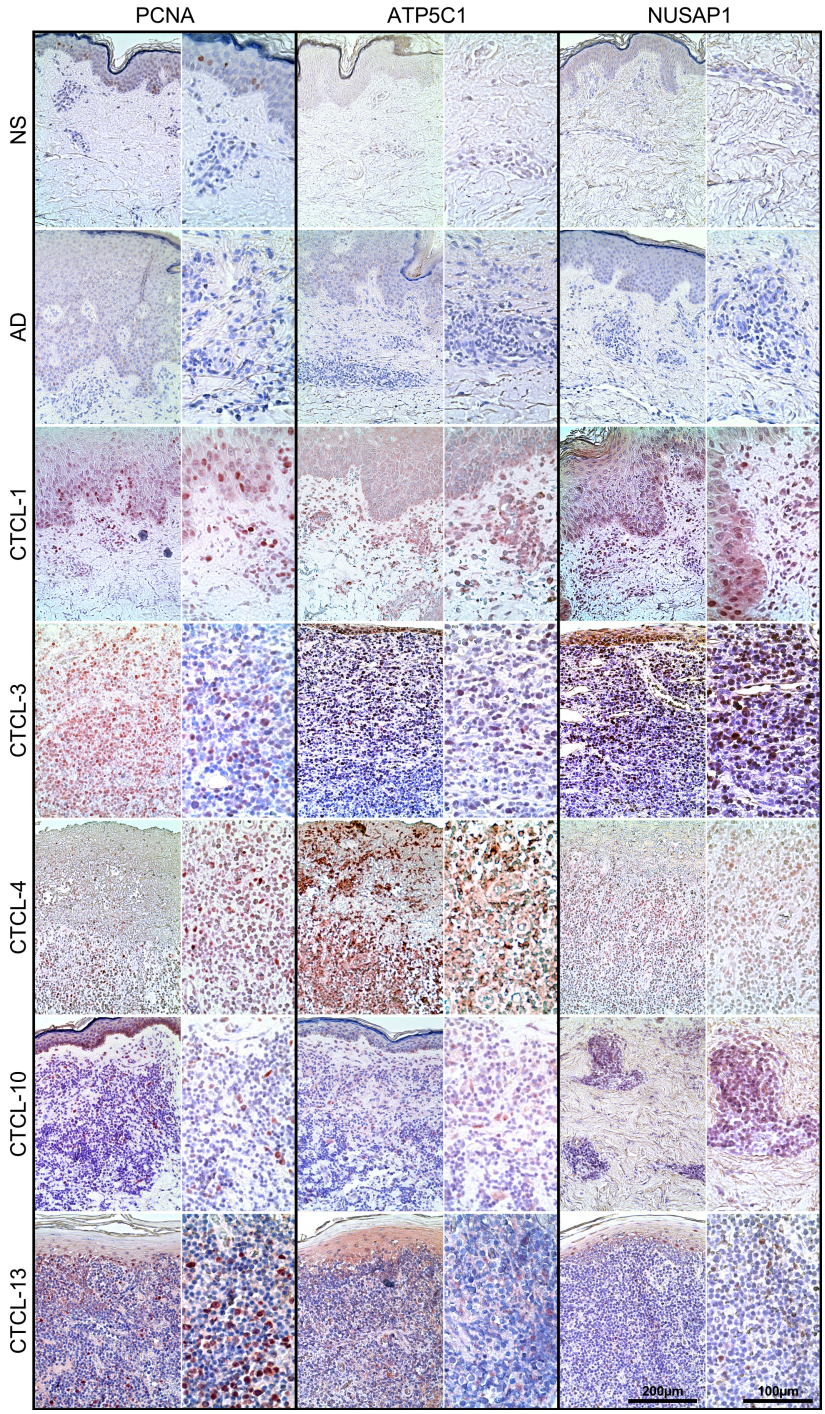

Supplementary Figure 5. Immunohistochemical stain from advanced-stage CTCL skin biopsies (n=5) of normal skin (NS, n=4), atopic dermatitis (AD, n=4), additional to the samples that were used in the scRNA-seq experiments, each at 200X (left) and 400X (right). (See Fig. 4). Immunohistochemistry procedures followed already established techniques(15).

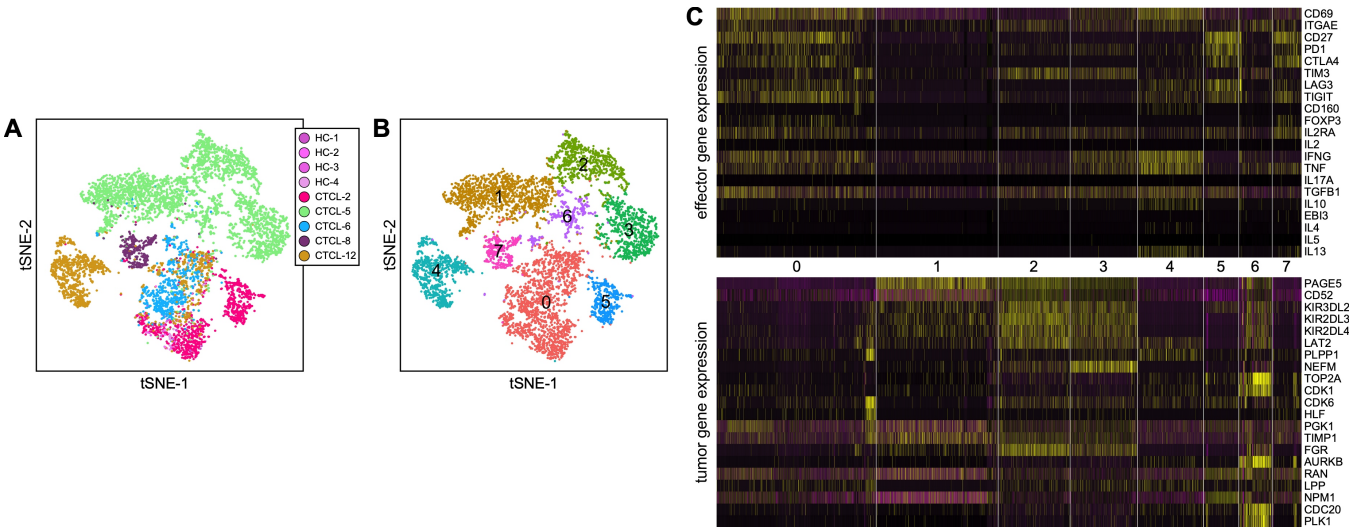

Supplementary Figure 6. (A) Transcriptomes of $CD3^{+}CD4^{+}$ T lymphocytes from individual CTCL tumors and normal skin samples (color coded by subject), revealing 8 discrete Louvain clusters **(B)**. **(C)** Gene expression from the clusters in (B), showing DE of co-inhibitory receptors and effector molecules (upper panel) and of tumor-associated genes (lower panel). Cluster numbers are indicated in the middle. Each column represents a cell.

Supplementary Table 1. (a) Demographic and clinical features of patients. CTCL-2, 5, 6, 8 and 12 were used in scRNA-seq experiments, while all were used in validation by immunohistochemistry (IHC). (b) Demographic features of normal donors. Samples from HC-1 to HC-4 were used for scRNA-seq while HC-5 to HC-8 were used for IHC.

a.

Patient	Age/ Sex	Stage*	TBSA (%patch, %plaque, %tumor)*	Year of dx	Study biopsy date	Blood involvement*	CD4/ CD8 *	TCR clone*	PET/CT *	Prior and current treatments (outcomes)	Outcome
CTCL-2	68/F	IVA T4NxB2M0	100% (erythro-dermic)	2015	5/2017	Large population of circulating CD4+/CD26- T-cells (3/2017).	25:1	+	FDG avid lymph nodes in the neck, axilla, and pelvis.	NBUVB (unable to tolerate), ongoing: topical steroids, bexarotene, and romidepsin	Stable disease.
CTCL-5	76/M	IIB T3N0B0M0	19% (10% patch, 5% plaque, 4% tumor)	2013	6/2017	Negative for blood involvement. Small T-cell clone detected on molecular studies (7/2016).	3:2	+	FDG avid cutaneous lesions in the chest, abdomen, bilateral lower extremities, and hand.	PUVA (initial improvement then recurrence), topical steroids (as needed), nitrogen mustard (progression), bexarotene (discontinued due to elevated triglycerides), LEB (progression), radiation therapy (progression), methotrexate (progression), Pralatrexate (progression and death)	CD8+ aggressive cytotoxic CTCL with disease progression and large cell transformation in 2016. Deceased, 2017.
CTCL-6	83/F	IIB T3NxB0M0	8.4% (1.1% patch, 5.5% plaque, 1.8% tumor)	2016	11/2017	Negative for blood involvement (11/2017).	2:1	+	Multifocal FDG cutaneous and lower extremity intra-muscular lesions throughout the body with hypermetabolic lymphadenopathy in the cervical, axillary, and pelvis region.	Nitrogen mustard (unable to adhere to application schedule, progression), bexarotene, pralatrexate, & LEB (progression and death)	Deceased, 2017.
CTCL-8	46/F	IIB T3N0B0M0	30% (29% patch/plaque, 1% tumor)	2005	11/2017	Negative for blood involvement (11/2016).	1:1	-	No evidence of lymphadenopathy or visceral disease.	Vorinostat (progression), NBUVB (progression), PUVA (progression), methotrexate (progression), IFN alpha (ongoing, progression), topical steroids (ongoing progression), nitrogen mustard (ongoing progression), bexarotene (ongoing, progression)	Disease progression.
CTCL-12	77/M	IVAT4NxM0B0	100% (94.5% patch, 4.5% plaque, 1% tumor)	2016	4/2018	Negative for blood involvement (3/2018).	2:1	+	Posterior neck subcutaneous lesion, and 2 bilateral FDG avid cervical lymph nodes concerning for malignant involvement. Low grade FDG uptake associated with skin thickening posterior to the left proximal tibia is seen.	Triamcinolone cream (patient discontinued due to difficulty with adherence), Valchlor (patient discontinued due to difficulty with adherence), bexarotene (patient discontinued due to difficulty with adherence), Romidepsin (current)	Large cell transformation in 2018. B-cell lymphocytosis of undetermined significance (small population of CD5/CD10 negative, kappa (bright) restricted B cells by flow)
CTCL-1	83/M	IVA T4NxB2M0	100% (erythrodermic)	2016	12/2016	Large population of circulating of CD4+/CD26- cells (12/2016).	15:1	+	Unavailable.	Interferon (discontinued due to neuropathy), PUVA (discontinued due to difficulty with his scheduling), bexarotene (discontinued due to slight elevation of LFTs), Extracorporeal photopheresis (ongoing)	Stable disease.
CTCL-3	70/M	IIB T3NxB0 M0	55% (50% patch, 5% plaque, 0.125% tumor)	2000	5/2017	No definitive evidence of blood involvement (7/2017).	2:1	+	Increased FDG uptake at the level of the right nipple (SUV 7.3). Stable bilateral axillary and inguinal lymph node FDG avidity that is possibly inflammatory in nature.	NBUVB (discontinued due to progression), interferon (discontinued due to fatigue, paresthesia, progression), Valchlor (current), clobetasol 0.05% ointment (current), bexarotene (discontinued due to progression) brentuximab (discontinued due to neuropathy & progression), AFM13 Affimed trial†† (ongoing)	Large cell transformation (CD30+) in 2017. Deceased, 2017.
CTCL-4	58/F	IIB T3NxM0B0	33.95% (25% patch, 3.45% plaque, 5.5% tumor)	2015	5/2017	Negative for blood involvement (5/2017).	3:1	-	FDG avid cutaneous thicken-ing in the left thigh and knee joint. FDG avid axillany and pelvic lymph nodes.	Romidepsin and Pralatrexate (progresion), light therapy (progression), AGS67E clinical trial‡‡ (ongoing), AFM 13 clinical trial†† (ongoing), undergoing allogenic bone marrow transplant	Transformed Cytotoxic mycosis fungoides (CD30+) diagnosed in 2017.
CTCL-10	63/F	IIB T3NxM0B0	2% (1.5% patch, 0.25% tumor)	2016	3/2018	Negative for blood involvement (11/2016).	3:1	-	None.	Triamcinolone gel (current), Valchlor (current)	Stable disease.
CTCL-13	48/F	IIB T3NxM0B0	5.5% (0.5% patch, 5% tumor)	2018	5/2018	Negative for blood involvement (4/2018).	1:1	-	Enlarged FDG active right thigh lymph nodes (SUV 3.7).	Brentuximab (current)	Improvement on current treatment. Last biopsy in 5/2018 was suggestive of MF with granuloma-tous features and focal large cell transformation with significant CD30 activity.

Abbreviations:
* Reported data is from the closest time point to the study biopsy date.
TBSA (total body surface area) at last follow-up visit with % patch, % plaque, and % tumor.
NBUVB: Narrowband UVB phototherapy
PUVA: psoralen long-wave ultraviolet radiation
LEB: Low-dose electron beam radiation
IFN: Interferon
‡TTI-621 (Trillium) clinical trial: NCT02663518 Phase I trial of TTI-621 for patients with hematologic malignancies and selected solid tumors; NCT02890368: Phase I trial of intratumoral injections of TTI-621 in subjects with relapsed and refractory solid tumors and mycosis fungoides
† EDO-S101 clinical trial: A Phase 1 Study to investigate the safety, pharmacokinetic profiles and the efficacy of EDO-S101, a first-in-class alkylating histone deacetylase inhibition (HDACi) fusion molecule, in relapsed/refractory hematologic malignancies (NCT02576496).
††Affirmed trial: Phase 1b/2a trial to investigate AFM13 as monotherapy in relapsed/refractory CD30-positive cutaneous lymphoma
‡‡AGS67E trial (NCT02175433): a phase 1 study evaluating safety, tolerability, and pharmacokinetics of escalating doses of AGS67E given as monotherapy in subjects with lymphoid refractory or relapsed lymphoid malignancies

b.

Subject	Sex	Age at Biopsy
HC-1	Male	64
HC-2	Female	48
HC-3	Male	54
HC-4	Male	61
HC-5	Female	58
HC-6	Male	60
HC-7	Male	51
HC-8	Female	48

Supplemental Table 2. Histology features of samples used in scRNA-seq and imaged in Figure 1a.

Patient No.	Histology and Immunohistochemistry
CTCL-2	The dermis contains a sparse perivascular mononuclear infiltrate. The epidermis shows mild acanthosis, slight spongiosis and foci of parakeratosis. There is mils lamellar fibrosis of the dermis. The nuclear atypia of the dermal lymphocytes is mild with few foci of exocytosis into the epidermis. Immunohistochemistry reveal CD4+, CD7- and CD8 largely negative infiltrate with significant CD4 predominance.
CTCL-5	The infiltrate is dense and involves the dermis and the subcutis, including superficial fat. The infiltrate is composed of enlarged, atypical lymphocytes with hyperchromatic nuclei and irregular nuclear contours. Lymphocytes are medium to large in size. There is prominent epidermotropism and papillary dermal edema. The epidermis shows mild spongiosis and hyperkeratosis with focal areas of parakeratosis containing serum. The atypical lymphocytes are CD3+, CD8+ and CD4-. A CD30 stain highlights few large lymphocytes in the dermal infiltrate. The histological findings are consistent with CD8+ aggressive cytotoxic cutaneous T-cell lymphoma with large cell transformation.
CTCL-6	An atypical lymphoid infiltrate with CD2, CD3, CD4 and CD5 immunostains mark the majority of the cells within the infiltrate. CD7 immunostain appears slightly down regulated. CD8 immunostain marks the minority of the cells within the infiltrate. CD79a and CD20 immunostain mark a very small minority of the cells in the infiltrate. CD30 immunostain as well as ALK1 immunostains are negative. CD56 immunostain is mostly negative. EBER is negative. T-cell receptor-beta gene rearrangement is positive for clonal TCR-beta gene rearrangement, consistent with a clonal lymphoid population in the sample. This represents a T-cell lymphoproliferative disorder/lymphoma (CD4 positive, CD30 negative).
CTCL-8	There is a significant psoriasiform hyperplasia; the single atypical lymphocytes infiltrate the epidermis, there are Langerhans cell rich microvesicles. The lymphocytes are mostly small to medium sized. There are a few large transformed-appearing cells, but they do not exceed more than 25% of the intraepidermal lymphocyte population. The dermal infiltrate is mostly perivascular, but there is some follicular involvement and a subtle granulomatous component. The cells are CD4+ CD7-, CD8 is significantly diminished.
CTCL-12	The skin biopsy demonstrates an atypical epidermotropic lymphocytic infiltrate with many lymphocytes with cerebriform appearance. Histopathology (not shown) revealed loss of CD2, CD5, betaF1 and both CD4 and CD8. There are numerous large atypical cells which exhibit CD30 positivity and an increased proliferation index of 30%, consistent with large cell transformation of mycosis fungoides. There are also granulomatous inflammatory features present, which usually signify worse prognosis and more aggressive clinical behavior, as well as resistance to topical therapies.

Supplementary Table 3. Gene expression signatures of individual tumor-specific clusters. We identified distinct gene expression signatures for each tumor-specific cluster, with examples listed in this table (see also Fig. 2D and Fig. S2).

Cluster	Gene types	Example genes
CTCL-2	eukaryotic initiation factors	eIF1, eIF2A, eIF3D, eIF3E, eIF3F, eIF3L, eIF4A3, eIF4E, eIF4G2
	Oncogenes	PIK3CA, MYC, FGFR1, GRB2
CTCL-5	NK-cell receptor and signaling molecules	KLRC2, CLEC12A, KIR2DL3, KIR3DL2, KIR3DL1, KIR2DL4, KIR2DL1, KLRC2, ATM, FCER1G, PIK3CD, PRKCA, PRKCB, RAC2
CTCL-6	tumor cell survival, proliferation, and metastasis	CDK6, HLF, LPP, MCTS1, NME1, CDCA7, PIM2, CLDND1, EML4, ANO1, PLPP1, IDH2, IDH3G, KRAS, PA2G4, PIK3R1, RB1, RRAS2, RASSF5, RXRA, TFDP1
CTCL-8	serpin, S100, and galectin families	SERPINB3, SERPINB4, S100A7, S100A8, S100A9, S100A14, LGALS7, LGALS7B, KRT17, KRT16, KRT6A
CTCL-12	increased cell motility and invasiveness	ATCB, ACTN4, ACTR2, ARF6, ARPC4, CDC42, MYL12A, PLCG2, IQGAP1, ZYX, TMPRSS3

Supplementary Table 4. List of the highly significant DE genes shown in the heat maps of Fig. 3C.

Supplementary Table 4a. CTCL-2

CTCL-2	p_val	avg_logFC	pct.1	pct.2	p_val_adj	cluster
PLK2	1.094E-75	1.445	0.555	0.089	1.843E-71	1
BRD2	1.336E-32	0.713	0.799	0.501	2.250E-28	1
NFKBIA	4.177E-62	1.307	0.856	0.627	7.035E-58	1
EIF4A3	9.478E-28	0.740	0.753	0.555	1.596E-23	1
GATA3	1.839E-20	0.795	0.737	0.352	3.097E-16	7
GATA3	5.978E-80	1.302	0.793	0.309	1.007E-75	1
SMC4	8.227E-14	0.629	0.519	0.246	1.386E-09	7
HES1	1.156E-30	1.285	0.314	0.075	1.947E-26	1
PSMB2	1.862E-03	0.288	0.288	0.160	1.000E+00	7
CCR7	4.974E-59	1.563	0.821	0.199	8.377E-55	7
CCR7	1.313E-57	1.257	0.632	0.179	2.212E-53	1
SET	5.092E-10	0.356	0.667	0.391	8.576E-06	7
SET	2.399E-08	0.303	0.552	0.388	4.040E-04	1
NR4A1	2.443E-70	1.234	0.813	0.391	4.114E-66	1
PCNA	4.592E-07	0.337	0.375	0.222	7.734E-03	1
CXCL13	3.318E-27	0.927	0.654	0.216	5.588E-23	7
CXCL13	9.214E-57	1.231	0.652	0.179	1.552E-52	1
RANBP1	3.135E-05	0.354	0.506	0.314	5.280E-01	7
TSC22D1	1.828E-49	1.225	0.485	0.121	3.078E-45	1
PPIA	9.944E-19	0.525	0.917	0.743	1.675E-14	7
PPIA	8.491E-19	0.375	0.866	0.737	1.430E-14	1
JUNB	1.560E-131	1.151	0.997	0.884	2.627E-127	1
HN1	6.522E-28	0.830	0.833	0.483	1.098E-23	7
HN1	1.416E-09	0.377	0.659	0.485	2.384E-05	1
SGK1	1.674E-39	1.053	0.452	0.108	2.820E-35	1
STMN1	2.740E-10	0.495	0.686	0.406	4.615E-06	7
STMN1	1.102E-06	0.280	0.572	0.403	1.856E-02	1
FAM43A	1.073E-10	0.420	0.365	0.140	1.807E-06	7
FAM43A	7.071E-39	1.042	0.425	0.110	1.191E-34	1
RAN	1.486E-06	0.320	0.801	0.600	2.502E-02	7
ARL4D	1.459E-03	0.415	0.295	0.169	1.000E+00	7
ARL4D	6.460E-40	1.030	0.472	0.126	1.088E-35	1
DUT	2.917E-05	0.258	0.346	0.186	4.912E-01	7
MYC	4.119E-30	1.030	0.485	0.210	6.937E-26	1
ATP5C1	1.985E-05	0.286	0.532	0.332	3.343E-01	7
ATP5C1	1.321E-06	0.271	0.488	0.323	2.225E-02	1
ZFAND2A	6.337E-31	0.979	0.488	0.179	1.067E-26	1
PPA1	1.232E-09	0.486	0.641	0.381	2.076E-05	7

SCG2	2.542E-33	0.930	0.405	0.096	4.281E-29	1
ACTG1	2.457E-18	0.381	0.936	0.908	4.138E-14	7
ACTG1	3.914E-38	0.528	0.957	0.902	6.593E-34	1
IGFL2	4.582E-12	0.278	0.372	0.154	7.716E-08	7
IGFL2	4.951E-43	0.914	0.478	0.116	8.339E-39	1
ANP32B	4.235E-06	0.274	0.603	0.388	7.132E-02	7
JUN	1.377E-35	0.896	0.779	0.442	2.320E-31	1
NUSAP1	7.034E-05	0.367	0.276	0.132	1.000E+00	7
IER2	1.283E-56	0.893	0.910	0.593	2.161E-52	1
NME1	1.601E-05	0.333	0.301	0.142	2.696E-01	7
NME1	2.529E-14	0.476	0.321	0.124	4.259E-10	1
RGS2	2.091E-28	0.884	0.682	0.410	3.521E-24	1
UQCRH	3.640E-04	0.273	0.686	0.521	1.000E+00	7
PGM2L1	1.292E-31	1.049	0.679	0.225	2.176E-27	7
PGM2L1	2.329E-38	0.879	0.585	0.203	3.922E-34	1
KPNB1	6.073E-06	0.378	0.436	0.243	1.023E-01	7
KPNB1	4.156E-08	0.278	0.401	0.232	6.999E-04	1
ID3	8.824E-28	0.865	0.565	0.241	1.486E-23	1
NR4A2	3.794E-39	0.849	0.803	0.515	6.391E-35	1
DNAJB1	2.606E-46	0.848	0.926	0.611	4.389E-42	1
FOS	5.796E-16	0.836	0.545	0.334	9.762E-12	1
GEM	2.505E-11	0.269	0.545	0.289	4.219E-07	7
GEM	2.571E-19	0.828	0.525	0.270	4.331E-15	1
TOB1	1.090E-33	0.827	0.709	0.392	1.836E-29	1
HSPB1	3.074E-33	0.819	0.793	0.535	5.177E-29	1
KLF6	9.949E-36	0.806	0.860	0.541	1.676E-31	1
BHLHE40	5.995E-34	0.768	0.589	0.225	1.010E-29	1
SOCS3	6.258E-31	0.760	0.686	0.343	1.054E-26	1

Supplementary Table 4b. CTCL-5

CTCL-5	p_val	avg_logFC	pct.1	pct.2	p_val_adj	cluster
TOP2A	0.000E+00	1.598	0.742	0.058	0.000E+00	4
ACTG1	4.175E-60	0.459	0.971	0.825	9.101E-56	4
UBE2C	0.000E+00	1.576	0.828	0.082	0.000E+00	4
PSMB2	6.089E-109	0.307	0.747	0.360	1.327E-104	4
HIST1H4C	6.164E-204	1.556	0.640	0.217	1.344E-199	4
PPA1	8.174E-84	0.296	0.226	0.390	1.782E-79	3
HMGB2	0.000E+00	1.479	0.926	0.413	0.000E+00	4
GLO1	1.732E-79	0.307	0.132	0.276	3.775E-75	3
ASPM	0.000E+00	1.433	0.707	0.048	0.000E+00	4
STMN1	2.407E-56	0.272	0.396	0.459	5.247E-52	3
STMN1	0.000E+00	1.267	0.930	0.405	0.000E+00	4
CENPF	3.155E-302	1.349	0.755	0.120	6.878E-298	4
DUT	4.329E-63	0.365	0.246	0.337	9.435E-59	3
DUT	6.174E-136	0.739	0.739	0.288	1.346E-131	4
AURKB	0.000E+00	1.233	0.702	0.030	0.000E+00	4
PCNA	7.535E-63	0.463	0.262	0.319	1.642E-58	3
PCNA	2.855E-93	0.467	0.665	0.278	6.223E-89	4
TUBB	6.185E-67	0.343	0.507	0.550	1.348E-62	3
TUBB	8.171E-244	1.157	0.913	0.509	1.781E-239	4
PPIA	1.370E-73	0.317	0.930	0.658	2.985E-69	4
KIAA0101	9.228E-35	0.271	0.214	0.256	2.011E-30	3
KIAA0101	2.481E-284	1.138	0.806	0.196	5.409E-280	4
MT1X	2.297E-66	0.425	0.323	0.404	5.006E-62	3
BIRC5	0.000E+00	1.127	0.716	0.050	0.000E+00	4
ANP32B	7.094E-101	0.337	0.672	0.298	1.546E-96	4
CKS1B	6.129E-293	1.113	0.805	0.211	1.336E-288	4
SMC4	2.973E-235	0.916	0.721	0.155	6.481E-231	4
TUBA1B	2.139E-255	1.088	0.955	0.589	4.663E-251	4
NUSAP1	0.000E+00	1.017	0.700	0.072	0.000E+00	4
MKI67	0.000E+00	1.065	0.715	0.071	0.000E+00	4
RAN	5.284E-109	0.395	0.854	0.513	1.152E-104	4
MAD2L1	0.000E+00	1.021	0.719	0.084	0.000E+00	4
ATP5C1	1.298E-86	0.287	0.262	0.416	2.829E-82	3
CDC20	3.709E-278	1.013	0.608	0.057	8.085E-274	4
HMGN1	3.084E-101	0.371	0.831	0.502	6.723E-97	4
PTTG1	1.582E-199	1.003	0.734	0.199	3.449E-195	4
SAR1A	7.023E-78	0.320	0.114	0.258	1.531E-73	3
HMGN2	5.881E-238	1.000	0.913	0.503	1.282E-233	4
PKM	1.846E-77	0.316	0.323	0.452	4.024E-73	3

GTSE1	0.000E+00	0.985	0.632	0.021	0.000E+00	4
NME1	6.921E-80	0.345	0.251	0.381	1.509E-75	3
CDK1	0.000E+00	0.935	0.655	0.041	0.000E+00	4
IFI6	3.166E-68	0.311	0.186	0.329	6.901E-64	3
CENPE	1.235E-281	0.933	0.560	0.035	2.692E-277	4
KPNB1	1.682E-91	0.271	0.639	0.277	3.665E-87	4
KPNA2	8.903E-166	0.911	0.739	0.234	1.941E-161	4
TYMS	6.386E-232	0.907	0.702	0.141	1.392E-227	4
PLK1	3.046E-293	0.903	0.511	0.020	6.638E-289	4
CCNB1	7.108E-267	0.881	0.527	0.034	1.549E-262	4
TUBB4B	2.756E-177	0.853	0.815	0.341	6.007E-173	4
HMGB1	8.882E-213	0.823	0.918	0.606	1.936E-208	4
NUF2	0.000E+00	0.817	0.629	0.025	0.000E+00	4
TIMP1	2.532E-80	0.528	0.438	0.521	5.518E-76	3
MT2A	1.936E-72	0.523	0.549	0.558	4.219E-68	3
EIF5A	8.691E-91	0.509	0.455	0.499	1.894E-86	3

Supplementary Table 4c. CTCL-6

CTCL-6	p_val	avg_logFC	pct.1	pct.2	p_val_adj	cluster
PLCG2	1.873E-24	1.242	0.367	0.114	3.607E-20	4
LSM5	3.987E-28	0.608	0.623	0.328	7.679E-24	4
NUCKS1	8.972E-52	0.897	0.754	0.341	1.728E-47	4
PSMB2	1.765E-15	0.409	0.577	0.341	3.399E-11	4
NME1	3.005E-54	0.878	0.658	0.312	5.787E-50	4
PPA1	3.651E-12	0.333	0.633	0.418	7.033E-08	4
SNRPE	4.100E-50	0.824	0.726	0.448	7.896E-46	4
HN1	6.268E-10	0.381	0.637	0.459	1.207E-05	4
PPIA	2.006E-48	0.627	0.829	0.770	3.864E-44	4
STMN1	1.106E-15	0.482	0.623	0.376	2.131E-11	4
KIAA0101	8.904E-43	0.781	0.555	0.157	1.715E-38	4
SKA2	1.470E-37	0.591	0.587	0.205	2.831E-33	4
SNHG25	6.025E-35	0.778	0.495	0.160	1.160E-30	4
PCNA	2.304E-23	0.561	0.534	0.232	4.437E-19	4
MIF	1.118E-36	0.776	0.733	0.503	2.154E-32	4
CKS1B	3.511E-22	0.591	0.498	0.215	6.763E-18	4
CLSPN	1.705E-42	0.728	0.456	0.107	3.284E-38	4
RANBP1	1.896E-19	0.471	0.623	0.344	3.652E-15	4
ANKRD36C	5.162E-29	0.722	0.445	0.137	9.942E-25	4
ANP32B	3.784E-08	0.285	0.644	0.476	7.288E-04	4

CENPF	9.243E-31	0.721	0.434	0.124	1.780E-26	4
SMC4	6.975E-14	0.362	0.548	0.304	1.343E-09	4
NDUFS6	1.871E-43	0.720	0.754	0.447	3.604E-39	4
NUSAP1	1.079E-10	0.356	0.331	0.152	2.078E-06	4
ANKRD36	7.860E-19	0.720	0.327	0.113	1.514E-14	4
PTPN7	2.025E-28	0.631	0.794	0.463	3.900E-24	4
IER5	4.067E-12	0.718	0.395	0.228	7.833E-08	4
ATP5C1	1.327E-09	0.317	0.569	0.402	2.556E-05	4
ATP5I	7.950E-30	0.718	0.701	0.434	1.531E-25	4
HMGN1	8.752E-08	0.318	0.633	0.520	1.686E-03	4
UQCRQ	3.607E-33	0.627	0.690	0.478	6.948E-29	4
MATK	7.984E-27	0.604	0.619	0.293	1.538E-22	4
ASPM	1.442E-30	0.709	0.349	0.077	2.778E-26	4
COX7B	7.671E-39	0.600	0.712	0.604	1.477E-34	4
PHF14	2.622E-33	0.698	0.566	0.208	5.050E-29	4
MZT2B	2.245E-31	0.603	0.701	0.509	4.323E-27	4
DUT	4.600E-26	0.697	0.616	0.314	8.860E-22	4
UQCRH	1.341E-17	0.401	0.705	0.592	2.584E-13	4
ATP5J2	2.381E-39	0.689	0.698	0.447	4.585E-35	4
KPNB1	2.285E-11	0.342	0.548	0.329	4.400E-07	4
LPAR6	1.136E-30	0.676	0.708	0.347	2.189E-26	4
CBX3	1.623E-37	0.674	0.733	0.455	3.125E-33	4
TESC	1.752E-32	0.649	0.534	0.192	3.375E-28	4
MRPL12	2.223E-35	0.646	0.580	0.221	4.281E-31	4
GADD45G	1.228E-17	0.643	0.356	0.131	2.366E-13	4
SNRPD1	7.939E-32	0.643	0.641	0.377	1.529E-27	4
SNRPF	1.545E-31	0.639	0.683	0.427	2.975E-27	4
PHYH	1.132E-15	0.639	0.302	0.130	2.180E-11	4
EBP	1.521E-38	0.635	0.662	0.405	2.930E-34	4
SSBP1	9.585E-32	0.632	0.637	0.395	1.846E-27	4

Supplementary Table 4d. CTCL-8

CTCL-8	p_val	avg_logFC	pct.1	pct.2	p_val_adj	cluster
DEK	2.035E-10	0.760	0.560	0.243	3.215E-06	3
TK1	7.664E-16	0.751	0.320	0.046	1.211E-11	3
IGFL2	4.917E-26	1.412	0.430	0.036	7.768E-22	3
PSMB2	4.753E-11	0.451	0.470	0.161	7.509E-07	3
KIAA0101	1.605E-24	1.340	0.450	0.053	2.535E-20	3
PPA1	2.012E-05	0.377	0.480	0.247	3.178E-01	3
HMGB2	4.930E-20	1.286	0.620	0.321	7.789E-16	3
CPM	1.134E-14	0.742	0.370	0.060	1.792E-10	3
TUBB	3.690E-18	1.164	0.680	0.349	5.830E-14	3
STMN1	2.449E-36	1.732	0.740	0.284	3.869E-32	3
HMGN2	4.017E-09	0.757	0.620	0.331	6.347E-05	3
DUT	1.897E-16	1.142	0.500	0.159	2.998E-12	3
HMGB1	9.472E-31	1.079	0.890	0.632	1.496E-26	3
PCNA	8.545E-14	0.921	0.480	0.130	1.350E-09	3
NTPCR	5.548E-18	0.733	0.430	0.073	8.766E-14	3
PPIA	4.533E-13	0.545	0.850	0.666	7.161E-09	3
GMFG	4.888E-18	0.970	0.770	0.376	7.723E-14	3
RANBP1	1.681E-12	0.726	0.580	0.263	2.656E-08	3
H1F0	1.158E-17	0.946	0.360	0.041	1.829E-13	3
ANP32B	4.463E-11	0.682	0.670	0.317	7.051E-07	3
CENPF	4.755E-13	0.941	0.340	0.058	7.512E-09	3
SMC4	5.324E-09	0.666	0.490	0.186	8.412E-05	3
HIST1H4C	1.492E-06	0.926	0.320	0.146	2.358E-02	3
NUSAP1	5.360E-09	0.694	0.320	0.079	8.468E-05	3
PASK	1.288E-15	0.924	0.440	0.088	2.035E-11	3
RAN	9.313E-09	0.569	0.730	0.472	1.471E-04	3
CORO1B	6.468E-16	0.924	0.670	0.243	1.022E-11	3
ATP5C1	1.085E-08	0.371	0.480	0.211	1.714E-04	3
CENPW	4.737E-15	0.728	0.310	0.035	7.484E-11	3
HMGN1	7.311E-08	0.593	0.670	0.412	1.155E-03	3
FYB	1.258E-11	0.849	0.740	0.409	1.987E-07	3
TOP2A	2.037E-12	0.723	0.260	0.029	3.219E-08	3
NDUFC2	1.898E-13	0.728	0.600	0.210	2.999E-09	3
SET	4.128E-07	0.626	0.550	0.274	6.522E-03	3
CKS1B	2.213E-12	0.847	0.430	0.115	3.496E-08	3
NME1	1.469E-06	0.262	0.300	0.119	2.321E-02	3
SPINT2	1.176E-14	0.837	0.450	0.110	1.858E-10	3
UQCRH	9.789E-06	0.528	0.650	0.408	1.547E-01	3
UBE2C	1.508E-11	0.816	0.260	0.033	2.383E-07	3

KPNB1	1.086E-05	0.260	0.390	0.186	1.716E-01	3
SSR4	6.376E-18	0.810	0.750	0.472	1.007E-13	3
FLNA	5.154E-11	0.802	0.630	0.297	8.142E-07	3
ABRACL	1.089E-12	0.798	0.660	0.291	1.721E-08	3
LEF1	3.565E-13	0.797	0.350	0.060	5.632E-09	3
CENPM	1.045E-16	0.781	0.400	0.063	1.651E-12	3
CARHSP1	6.046E-11	0.780	0.520	0.196	9.553E-07	3
GIMAP7	7.267E-11	0.777	0.540	0.198	1.148E-06	3
PGM2L1	2.282E-15	0.775	0.640	0.222	3.605E-11	3
ATP5L	9.899E-18	0.770	0.810	0.605	1.564E-13	3
MKI67	1.255E-13	0.763	0.330	0.049	1.983E-09	3

Supplementary Table 4e. CTCL-12

CTCL-12	p_val	avg_logFC	pct.1	pct.2	p_val_adj	cluster
HIST1H4C	7.227E-46	2.052	0.743	0.164	1.246E-41	7
KIF20B	7.724E-24	0.884	0.392	0.067	1.331E-19	7
UBE2C	1.641E-170	1.920	0.689	0.018	2.828E-166	7
SKA2	4.502E-21	0.848	0.405	0.078	7.760E-17	7
KIAA0101	1.442E-122	1.866	0.730	0.042	2.485E-118	7
ASF1B	1.138E-93	0.894	0.378	0.010	1.962E-89	7
HMGB2	5.260E-42	1.707	0.878	0.280	9.066E-38	7
RPA3	3.755E-22	0.830	0.595	0.164	6.472E-18	7
TUBB	3.264E-33	1.657	0.824	0.338	5.626E-29	7
STMN1	5.205E-42	1.486	0.730	0.160	8.971E-38	7
TK1	2.590E-98	0.899	0.446	0.014	4.465E-94	7
DUT	4.408E-22	1.054	0.595	0.173	7.598E-18	7
AURKB	2.472E-155	1.464	0.568	0.011	4.260E-151	7
PCNA	2.798E-27	0.999	0.500	0.097	4.823E-23	7
MKI67	6.190E-130	1.450	0.649	0.026	1.067E-125	7
CENPM	3.189E-51	0.743	0.392	0.029	5.497E-47	7
TYMS	1.209E-112	1.445	0.635	0.032	2.084E-108	7
RANBP1	9.886E-20	0.887	0.676	0.217	1.704E-15	7
UBE2S	1.626E-16	0.945	0.622	0.221	2.803E-12	7
ANP32B	1.173E-19	0.821	0.689	0.248	2.021E-15	7
TUBA1B	4.777E-21	1.343	0.770	0.365	8.234E-17	7
SMC4	6.210E-17	0.607	0.405	0.091	1.070E-12	7
CENPF	5.873E-82	1.268	0.486	0.026	1.012E-77	7
NUSAP1	8.732E-85	1.432	0.595	0.041	1.505E-80	7
ASPM	1.992E-88	1.189	0.405	0.013	3.433E-84	7

RAN	4.815E-13	0.726	0.757	0.375	8.299E-09	7
HMGB1	8.894E-25	1.147	0.905	0.612	1.533E-20	7
CENPN	7.262E-60	0.805	0.378	0.021	1.252E-55	7
HMGN2	6.474E-25	1.119	0.797	0.325	1.116E-20	7
HMGN1	2.648E-07	0.437	0.730	0.477	4.565E-03	7
BIRC5	3.803E-150	1.114	0.527	0.009	6.556E-146	7
MZT2B	1.775E-16	0.793	0.838	0.446	3.059E-12	7
MT2A	4.351E-20	1.107	0.946	0.523	7.500E-16	7
NUCKS1	4.775E-22	0.726	0.595	0.155	8.230E-18	7
CDKN3	3.394E-114	1.092	0.486	0.014	5.850E-110	7
MCM7	1.879E-28	0.886	0.419	0.064	3.238E-24	7
CKS1B	1.466E-52	1.082	0.554	0.064	2.528E-48	7
SMC2	9.865E-53	0.913	0.378	0.026	1.700E-48	7
GTSE1	3.558E-147	1.079	0.432	0.004	6.132E-143	7
CENPW	1.448E-47	0.796	0.392	0.032	2.495E-43	7
ZWINT	2.292E-116	1.076	0.486	0.013	3.950E-112	7
NUDT1	5.204E-51	1.074	0.649	0.089	8.969E-47	7
CDT1	7.821E-70	0.936	0.392	0.019	1.348E-65	7
RRM2	1.093E-114	1.018	0.446	0.010	1.883E-110	7
DEK	3.507E-24	0.915	0.649	0.182	6.044E-20	7
TOP2A	4.918E-122	0.996	0.473	0.011	8.476E-118	7
CDK1	3.258E-111	0.981	0.500	0.016	5.616E-107	7
H2AFZ	1.370E-18	0.973	0.838	0.475	2.361E-14	7
CDC20	2.722E-52	0.967	0.338	0.020	4.692E-48	7
CDCA5	1.114E-118	0.881	0.405	0.006	1.921E-114	7

Supplementary Table 5. Counts of $CD3^{+}CD8^{+}$ cells contributing to each cluster from the different tumors and normal samples (Figure 5).

	Cluster 0	Cluster 1	Cluster 2	Cluster 3	Cluster 4	Cluster 5	Cluster 6
Normals	0	32	0	0	0	0	0
CTCL-2	0	166	0	0	0	0	1
CTCL-5	658	75	579	0	0	187	127
CTCL-6	1	258	2	344	291	1	10
CTCL-8	0	53	0	0	0	3	1
CTCL-12	3	75	2	0	0	0	0
Totals	**662**	**659**	**583**	**344**	**291**	**191**	**139**